PHYSOR 2012 – Advances in Reactor Physics – Linking Research, Industry, and Education
Knoxville, Tennessee, USA, April 15-20, 2012, on CD-ROM, American Nuclear Society, LaGrange Park, IL (2012)

CASMO5/TSUNAMI-3D SPENT NUCLEAR FUEL REACTIVITY UNCERTAINTY ANALYSIS

Rodolfo Ferrer and Joel Rhodes
Studsvik Scandpower, Inc.
504 Shoup Ave., Suite 201, Idaho Falls, ID 83402
rodolfo.ferrer@studsvik.com; joel.rhodes@studsvik.com

Kord Smith
Department of Nuclear Science and Engineering
Massachusetts Institute of Technology
77 Massachusetts Avenue, Cambridge, MA 02139
kord@mit.edu

ABSTRACT

The CASMO5 lattice physics code is used in conjunction with the TSUNAMI-3D sequence in ORNL's SCALE 6 code system to estimate the uncertainties in hot-to-cold reactivity changes due to cross-section uncertainty for PWR assemblies at various burnup points. The goal of the analysis is to establish the multiplication factor uncertainty similarity between various fuel assemblies at different conditions in a quantifiable manner and to obtain a bound on the hot-to-cold reactivity uncertainty over the various assembly types and burnup attributed to fundamental cross-section data uncertainty.

Key Words: Spent Fuel, Uncertainty Analysis, CASMO, TSUNAMI.

1. INTRODUCTION

Benchmarks for quantifying fuel sub-batch reactivity depletion uncertainty have been recently developed by Studsvik Scandpower for the Electric Power Research Institute (EPRI) [1, 2, 3]. The experimental biases, derived for the CASMO lattice physics code, were used to develop the experimental benchmarks. However, the resulting experimental biases correspond to CASMO Hot Full Power (HFP) conditions. The extension of these results from HFP to cold conditions is performed in order to obtain an uncertainty bound on the HFP-to-cold reactivity due to fundamental cross-section uncertainty.

The TSUNAMI [4] analysis sequences are capable of estimating the impact of cross-section uncertainties in a critical system's multiplication factor, denoted *k*, by propagating uncertainties through the use of sensitivity coefficients and first-order perturbation theory. The sensitivity coefficients represent a change in the system's response due to a change in the input parameters. In particular the TSUNAMI approach uses explicit ($S_{k,\Sigma_{x,g}}$) and implicit (S_{k,ω_i}) sensitivity coefficients, which are defined as follows

$$S_{k,\Sigma_{x,g}} = \frac{\Sigma_{x,g}}{k}\frac{\partial k}{\partial \Sigma_{x,g}} \quad (1)$$

$$S_{\Sigma_{x,g},\omega_i} = \frac{\omega_i}{\Sigma_{x,g}}\frac{\partial \Sigma_{x,g}}{\partial \omega_i} \quad (2)$$

where $\Sigma_{x,g}$ is the macroscopic cross-section for reaction *x* and group *g*, and ω_i is the nuclear data component of some isotope *i*. The implicit sensitivity coefficient is propagated to *k* through the use of the chain rule for derivatives. The response uncertainty is obtained by summing all the contributions to the system response from the uncertainties through the sensitivity coefficients and covariance data [5].

In addition to computing uncertainties in the multiplication factor, the SCALE 6 code system [6] is capable of computing a correlation coefficient, which is representative of the similarity (in terms of uncertainty) between two critical systems. The computation of the correlation coefficient is performed by the TSUNAMI-IP sequence in SCALE 6, which uses the sensitivity data generated by TSUNAMI, along with nuclear covariance data, to assess the similarity between two systems.

2. CASMO5/TSUNAMI-3D UNCERTAINTY ANALYSIS

CASMO5 [7] was used to perform the lattice depletion and branch calculations for a variety of fuel assemblies. CASMO5 was employed, rather than CASMO-4 [8], because its library includes all nuclides needed to avoid the use of lumped fission products, and hence more consistent with SCALE 6. In order to obtain the burnup-dependent isotopic compositions in each fuel and burnable rod for the TSUNAMI-3D calculation, a script was developed which used the CASMO5 lattice geometry, temperature, and region-wise isotopic composition to generate suitable SCALE 6 input files. This process was applied to all lattice types and branch conditions for selected burnup points.

A 17 x 17 Westinghouse Robust Fuel Assembly (RFA) fuel assembly with 5% enrichment, 104 Integral Fuel Burnable Absorbers (IFBA), and 20 Wet Annular Burnable Absorbers (WABA) was selected as a base case. A case matrix was constructed for different enrichments (3.5 % and 4.25 %), number of burnable absorbers (128 IFBA, 24 WABA), and fuel pin radius (smaller than nominal) for a total of five lattice cases. All five lattice cases were depleted with CASMO5 to 60 GWd/T and "branched" from HFP to six other conditions (HFP No Xenon, Hot Zero Power, Cold 1000 ppm boron, Cold no boron, Cold no boron with 100-hour decay, and simplified rack geometry) at eight burnup points (0.0, 0.5, 10, 20, 30, 40, 50, and 60 GWd/T).

Since the 44-group covariance library [9] in SCALE-6 is in multi-group format, the TSUNAMI-3D sequence uses the unresolved (BONAMIST) and resolved resonance self-shielding modules (NITAWLST or CENTRMST) to produce problem-specific multi-group cross-section and sensitivity libraries for the multi-group transport calculation. Cross-sections in each fuel pin region (with unique isotopic number densities) were self-shielded in the TSUNAMI calculation. The NITAWLST module was selected over CENTRMST module to perform the resolved

resonance self-shielding calculation in order to keep the overall run time short enough to analyze the complete case matrix. Unfortunately, the lower-accuracy NITAWL treatment (relative to CENTRM) is also limited to older ENDF libraries; hence the 238-group ENDF/B-V5 library was selected for this analysis. Forward and adjoint multi-group transport calculations in TSUNAMI-3D are performed by the KENO multi-group Monte Carlo code. Ideally, continuous-energy Monte Carlo would be used since significant computational resources are already expended in the KENO multi-group calculation. However, a multi-group solution is necessary in order to compute the sensitivities given that the covariance library is in multi-group format. Finally, the TSUNAMI-3D KENO-VI sequence was chosen to take advantage of the ¼ assembly geometry symmetry. Once forward and adjoint transport computations were completed, the SAMS module was used to generate problem-specific uncertainty data and sensitivity library to be used for post-processing. This library is read by TSUNAMI-IP to generate correlation coefficients.

3. UNCERTAINTY ANALYSIS RESULTS

TSUNAMI-3D computed the uncertainty data for the lattice multiplication factors as a function of various lattices, conditions, and burnups. The uncertainty results for the base lattice at HFP and cold conditions as a function of burnup are shown in Table I.

Table I. Multiplication Factor Uncertainty (2-sigma) as Function of Burnup

Burnup (GWd/T)	0.5	10.	20.	30.	40.	50.	60.
k-infinity Hot	1.02068	1.08597	1.08298	1.03600	0.97772	0.92176	0.87200
Uncertainty (pcm)	1034	1104	1211	1265	1295	1311	1323
k-infinity Cold	1.16103	1.23979	1.25419	1.21057	1.14557	1.07995	1.01883
Uncertainty (pcm)	1015	1087	1209	1281	1326	1361	1388

The hot-to-cold reactivity uncertainties can be obtained from the data shown above and the correlation coefficient obtained from the evaluation of the covariance matrix between the two states. The results from this analysis are shown in Table II. The propagation of uncertainties as independent variables (without correlation) is also shown to illustrate the importance of the correlation between hot-to-cold conditions on the uncertainty.

Table II. HFP to Cold Reactivity Uncertainty (2-sigma) as Function of Burnup

Burnup (GWd/T)	0	0.5	10.	20.	30.	40.	50.	60.
Uncertainty (pcm)	347	427	459	508	527	530	521	509
Uncertainty (pcm)*	1479	1476	1580	1748	1840	1893	1926	1949

* Propagation of uncertainty such that covariance (k-hot, k-cold) = 0

The inclusion of the correlation reduces the uncertainty by about a factor of four. The two states are expected to be highly correlated due to the fact that there is no burnup difference, and isotopic compositions remain the same.

For any lattice and depletion point, the similarity in the uncertainty between different physical conditions can be quantified by the use of the correlation coefficient. A correlation coefficient of unity indicates perfect similarity (identical systems) while a correlation of zero indicates negligible similarity. In the following analysis, the correlation factor shows the similarity between different states and lattice types at a fixed burnup step.

A summary of the correlation coefficients is shown in Table A.I (Appendix A) for the five lattice types between nominal (HFP) and branch conditions. The correlation factors corresponding to the nominal and branch conditions for the *base lattice case* in Table A.I are depicted in Figure 1 below in order to facilitate the discussion. The correlations corresponding to nominal HFP conditions are unity because identical conditions are being compared. **The base lattice (and all other lattices in Table A.I) shows a very high degree of similarity between HFP and various cold conditions, at all burnup points** – even though xenon, fuel temperature, coolant temperature, boron concentration, and local rack conditions change dramatically. (For the rack case, a simplified uniform rack has been assumed with a pitch of 22.5 cm, a .1 cm thick stainless steel can, a .0625 cm thick borated aluminum poison sheet having a width of 19 cm, and a ^{10}B areal density of 0.006 gm/cm^2.)

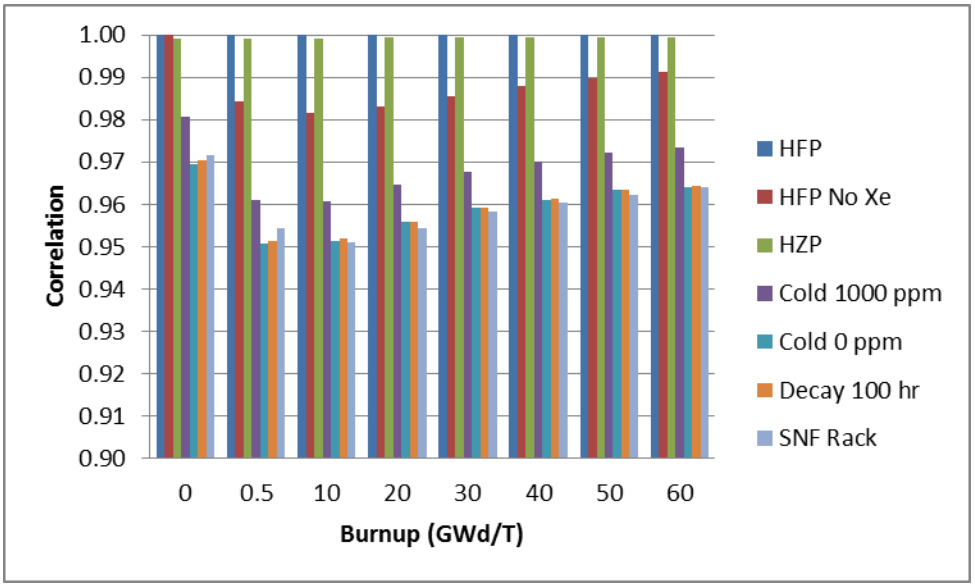

Figure 1. Correlation factors between nominal HFP and branch conditions at fixed burnup steps for base lattice.

A second comparison between different lattice types was performed at HFP, cold (no boron, 100-hour decay), and cold rack conditions, and the results are presented in Tables A.II and A.III. The correlation factors corresponding to the nominal HFP state in Tables A.II and A.III are depicted in Figures 2 and 3, respectively, to facilitate the discussion. In Figure 2 and Table A.II, all correlation coefficients are computed relative to the base case at zero burnup. It can be seen that the similarity changes significantly with burnup as the isotopics of the fuel change from fresh uranium to the higher actinides and fission products. Figure 3 and Table A.III displays the correlation coefficients for the same cases measured relative to the base case at each burnup

state. These results indicate **an extremely high degree of similarity exists between all lattice types – at each burnup point**. This is important for spent fuel uncertainty analysis, as biases in reactivity decrement as a function of burnup are derived directly from reactor measurements, and only the uncertainty from HFP reactor conditions to cold spent fuel pool/cask conditions is needed from the TSUNAMI analysis.

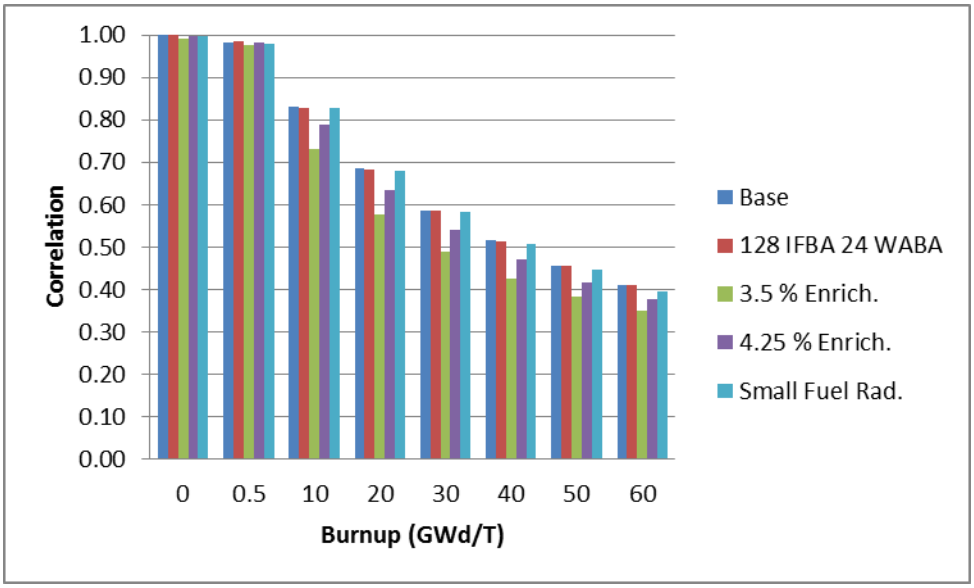

Figure 2. Correlation factors between base lattice at zero burnup and various lattice cases at fixed nominal HFP.

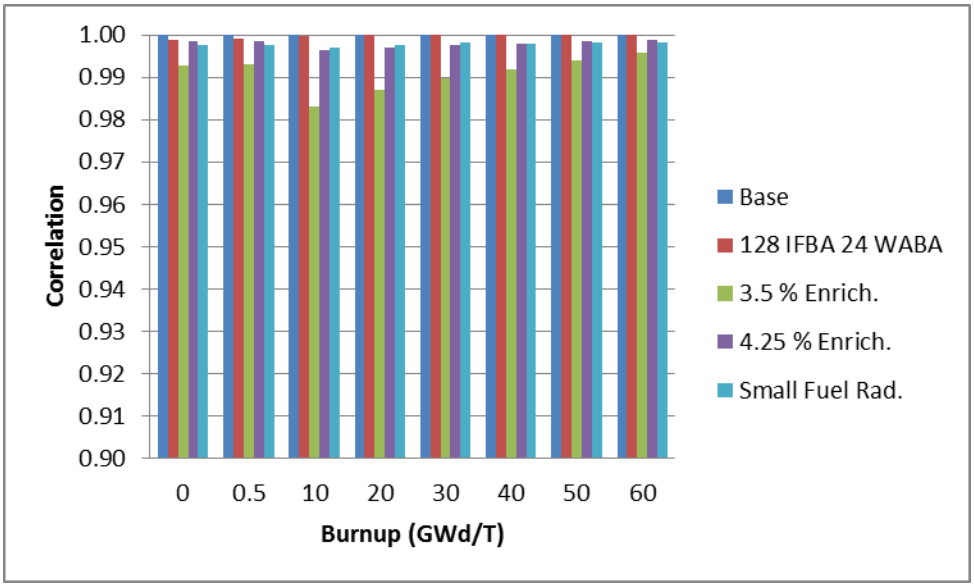

Figure 2. Correlation factors between base lattice and various lattice cases at nominal HFP and fixed burnup steps.

Finally, the quantities of direct interest in this study, reactivity and reactivity uncertainty between HFP and cold (no boron, 100-hour decay), are displayed in Table III, for all lattice types. The maximum 2-sigma reactivity uncertainty (due to cross-section data uncertainties) over all lattice types and burnup points is 555 pcm. Table IV displays the corresponding reactivity and reactivity uncertainty between HFP and Cold simplified SFP rack conditions. The uncertainties displayed in Table IV are uniformly lower than those in Table III, indicating that the cross-section data uncertainties are less important in the SFP absorbing rack geometry. This is a reflection of the fact that the hardening of the spectrum caused by the SFP rack actually makes the spectrum closer to the lattice spectrum at HFP conditions than to the lattice spectrum at cold conditions. Consequently, the **impacts of cross section uncertainties on the reactivity changes from HFP-to-cold conditions are very similar in operating reactor conditions and cold rack geometry.**

Table III. HFP to Cold Uncertainty Matrix (2-sigma) at Cold Conditions

		Burnup (GWd/T)							
	Conditions	**0.0**	**0.5**	**10.**	**20.**	**30.**	**40.**	**50.**	**60.**
Base	**Reactivity (pcm)**	9867	11843	11425	12605	13919	14986	15891	16527
	Uncertainty	347	427	459	508	527	530	521	509
128 IFBA 24 WABA	**Reactivity (pcm)**	9977	11927	11367	12556	13916	15009	15888	16612
	Uncertainty	337	403	450	508	533	531	521	512
3.5 % Enrichment	**Reactivity (pcm)**	12703	14810	13078	14402	15525	16266	16734	17034
	Uncertainty	365	437	498	555	550	537	518	500
4.25 % Enrichment	**Reactivity (pcm)**	11069	13112	12209	13469	14747	15699	16415	16931
	Uncertainty	350	434	473	529	540	534	520	508
Small Fuel Radius	**Reactivity (pcm)**	10205	12262	11602	12658	13981	14991	15849	16473
	Uncertainty	322	402	442	497	524	518	509	492

Table IV. HFP to Cold Uncertainty Matrix (2-sigma) in Rack Geometry

		Burnup (GWd/T)							
	Conditions	**0.0**	**0.5**	**10.**	**20.**	**30.**	**40.**	**50.**	**60.**
Base	**Reactivity (pcm)**	-10145	-8018	-6291	-4658	-4002	-4097	-4601	-5344
	Uncertainty	222	287	324	353	358	356	349	339
128 IFBA 24 WABA	**Reactivity (pcm)**	-10405	-8323	-6684	-4858	-4094	-4130	-4626	-5347
	Uncertainty	212	274	317	352	364	354	346	341
3.5 % Enrichment	**Reactivity (pcm)**	-12437	-9905	-7382	-5715	-5839	-6687	-7688	-8688
	Uncertainty	204	266	330	364	357	349	343	337
4.25 % Enrichment	**Reactivity (pcm)**	-11101	-8772	-6740	-5028	-4684	-5123	-5916	-6873
	Uncertainty	211	279	327	357	359	350	342	337
Small Fuel Radius	**Reactivity (pcm)**	-10594	-8366	-6705	-5185	-4676	-5046	-5851	-7075
	Uncertainty	201	274	315	348	356	345	336	327

Since the uncertainty changes in Table IV may be dependent on the actual rack design, it is conservative to use the uncertainties computed directly at cold conditions – without taking any credit for reduction in uncertainty that arise in the Spent Fuel Pool or cask geometry. Taking the largest HFP-to-cold uncertainty change from any lattice in Table III and assuming it applied to all fuel lattices one obtains the conservative burnup dependent uncertainties displayed in Table V.

Table V. HFP to Cold Uncertainty Matrix (2-sigma) vs. Burnup

Burnup (GWd/T)	**0.0**	**0.5**	**10.**	**20.**	**30.**	**40.**	**50.**	**60.**
Uncertainty (pcm)	365	437	498	555	550	537	521	512

However, the uncertainty for fresh fuel in cold SFP or cask conditions will actually be determined for specific applications through the evaluation of a large set of cold criticals, and there is no reason to include reactivity uncertainty due to fresh fuel cross-section uncertainties. Consequently, statistically subtracting the smallest fresh fuel uncertainty (322 pcm) from the other uncertainties in Table V, one obtains the hot-to-cold reactivity uncertainties (due to cross-section uncertainties) as a function of fuel depletion, as displayed in Table VI.

Table VI. HFP to Cold Additional Uncertainty Matrix (2-sigma) vs. Burnup

Burnup (GWd/T)	**0.0**	**0.5**	**10.**	**20.**	**30.**	**40.**	**50.**	**60.**
Uncertainty (pcm)	172	295	380	452	446	430	410	398

3. CONCLUSIONS

The CASMO5/TSUNAMI-3D analysis has demonstrated a high degree of correlation between PWR fuel assemblies such that the nuclear data uncertainties are nearly independent of assembly design and enrichment. Since the bias in reactivity is accounted for at HFP conditions, which takes into account the uncertainty due to depletion, only hot-to-cold uncertainties are needed in order to obtain an estimate of the reactivity uncertainty for spent nuclear fuel. The CASMO5/TSUNAMI-3D analysis demonstrated that the extremely high correlation of reactivities between hot-to-cold conditions results in additional uncertainties for extending HFP reactivity decrement measurements to cold conditions of less than 460 pcm over the range of burnups from 0 to 60 GWd/T.

Recommendations for future work include the extension of this analysis to full-core geometries, which is possible through the use of the CASMO5 MxN option and the TSUNAMI-3D sequence. Further comparisons between NITAWLST and CENTRM and various SCALE 6 cross-section libraries may be of interest in order to determine the impact upon the reactivity uncertainty results.

REFERENCES

1. K. S. Smith, S. Tarves, T. Bahadir, R. Ferrer, *Benchmarks for Quantifying Fuel Reactivity Depletion Uncertainty*, Electric Power Research Institute (EPRI) 1022909, Palo Alto, CA (2011).
2. S. Tarves, "Determination of the Uncertainty in the Delta K of Depletion Using PWR Power Distribution Measurements," *International Conference on Nuclear Criticality (ICNC 2011)*, Edinburgh, Scotland, UK, Sept. 19-22 (2011).
3. D. B. Lancaster, "Utilization of the EPRI Delta K of Depletion Benchmarks in PWR Spent Fuel Pool Criticality Analysis," *International Conference on Nuclear Criticality (ICNC 2011)*, Edinburgh, Scotland, UK, Sept. 19-22 (2011).
4. M. L. Williams, B. T. Rearden, "SCALE-6 Sensitivity/Uncertainty Methods and Covariance Data," IDOC 11583.
5. B. L. Broadhead, B. T. Rearden, C. M. Hopper, J. J. Wagschal, C. V. Parks, "Sensitivity- and Uncertainty-Based Criticality Safety Validation Techniques," *Nucl. Sci. Eng.*, **146**, pp. 340-366 (2004).
6. *SCALE: A Modular Code System for Performing Standardized Computer Analyses for Licensing Evaluation*, ORNL/TM-2005/39, Version 6, Vols. I-III, Oak Ridge National Laboratory, Oak Ridge, TN (2009).
7. J. Rhodes, K. Smith, D. Lee, "CASMO-5 Development and Applications," *Advances in Nuclear Analysis and Simulation (PHYSOR 2006)*, Vancouver, BC, Canada, Sept. 10-14, (2006).
8. K. Smith, J. Rhodes, "CASMO-4 Characteristic Methods for Two Dimensional PWR and BWR Core Calculations," *Trans. Am. Nucl. Soc.*, **83**, 322 (2000).
9. M. L. Williams, D. Wiarda, G. Arbanas, B. L. Broadhead, *Scale Nuclear Data Covariance Library*, ORNL/TM-2005/39, Version 6, Vol. III Sect. M19, Oak Ridge National Laboratory, Oak Ridge, TN (2009)

APPENDIX A

Table A.I. Correlation Coefficients, c_k, Between Reactor Conditions by Lattice and Burnup

		Burnup (GWd/T)							
	Conditions	**0.0**	**0.5**	**10.**	**20.**	**30.**	**40.**	**50.**	**60.**
Base	**HFP**	1	1	1	1	1	1	1	1
	HFP No Xe	1	0.9843	0.9817	0.9831	0.9854	0.9878	0.9898	0.9914
	HZP	0.9992	0.9992	0.9992	0.9995	0.9994	0.9994	0.9995	0.9995
	Cold 1000 ppm	0.9807	0.9609	0.9608	0.9646	0.9678	0.9702	0.9723	0.9734
	Cold 0 ppm	0.9694	0.9506	0.9514	0.9560	0.9592	0.9611	0.9634	0.9640
	Decay 100 hr	0.9705	0.9512	0.9519	0.9558	0.9591	0.9613	0.9633	0.9643
	SNF Rack	0.9717	0.9543	0.9510	0.9543	0.9582	0.9605	0.9623	0.9641
128 IFBA 24 WABA	**HFP**	1	1	1	1	1	1	1	1
	HFP No Xe	1	0.9863	0.9829	0.9835	0.9856	0.9879	0.9899	0.9914
	HZP	0.9993	0.9993	0.9992	0.9993	0.9994	0.9994	0.9995	0.9994
	Cold 1000 ppm	0.9799	0.9638	0.9616	0.9648	0.9677	0.9703	0.9724	0.9734
	Cold 0 ppm	0.9708	0.9526	0.9525	0.9558	0.9587	0.9617	0.9638	0.9643
	Decay 100 hr	0.9702	0.9548	0.9531	0.9559	0.9585	0.9614	0.9634	0.9641
	SNF Rack	0.9725	0.9559	0.9518	0.9547	0.9572	0.9611	0.9630	0.9638
3.5 % Enrichment	**HFP**	1	1	1	1	1	1	1	1
	HFP No Xe	1	0.9851	0.9828	0.9853	0.9884	0.9907	0.9923	0.9934
	HZP	0.9994	0.9992	0.9993	0.9984	0.9996	0.9995	0.9994	0.9995
	Cold 1000 ppm	0.9799	0.9617	0.9637	0.9675	0.9714	0.9726	0.9738	0.9744
	Cold 0 ppm	0.9670	0.9482	0.9521	0.9569	0.9603	0.9622	0.9631	0.9641
	Decay 100 hr	0.9669	0.9482	0.9526	0.9566	0.9608	0.9622	0.9632	0.9639
	SNF Rack	0.9734	0.9565	0.9538	0.9572	0.9612	0.9630	0.9641	0.9649
4.25 % Enrichment	**HFP**	1	1	1	1	1	1	1	1
	HFP No Xe	1	0.9842	0.9818	0.9838	0.9867	0.9891	0.9910	0.9924
	HZP	0.9994	0.9993	0.9995	0.9995	0.9995	0.9995	0.9995	0.9995
	Cold 1000 ppm	0.9808	0.9617	0.9618	0.9659	0.9698	0.9718	0.9734	0.9740
	Cold 0 ppm	0.9700	0.9504	0.9512	0.9558	0.9598	0.9625	0.9636	0.9641
	Decay 100 hr	0.9696	0.9490	0.9524	0.9565	0.9602	0.9622	0.9636	0.9639
	SNF Rack	0.9730	0.9547	0.9517	0.9560	0.9596	0.9624	0.9640	0.9645

Small Pin Radius	**HFP**	1	1	1	1	1	1	1	1
	HFP No Xe	1	0.9816	0.9781	0.9797	0.9827	0.9857	0.9882	0.9904
	HZP	0.9992	0.9992	0.9994	0.9995	0.9995	0.9996	0.9996	0.9996
	Cold 1000 ppm	0.9814	0.9608	0.9589	0.9618	0.9652	0.9690	0.9712	0.9728
	Cold 0 ppm	0.9709	0.9498	0.9488	0.9521	0.9556	0.9591	0.9616	0.9628
	Decay 100 hr	0.9709	0.9510	0.9497	0.9530	0.9555	0.9596	0.9614	0.9630
	SNF Rack	0.9743	0.9536	0.9486	0.9513	0.9548	0.9590	0.9615	0.9632

Table A.II. Correlation Coefficients, c_k, Between Lattice Types (Relative to Base Lattice at 0 GWd/T)

		Burnup (GWd/T)							
	Lattice	**0.0**	**0.5**	**10.**	**20.**	**30.**	**40.**	**50.**	**60.**
HFP	**Base**	1	0.9837	0.8321	0.6849	0.5867	0.5149	0.4567	0.4100
	128 I 24 W	0.9989	0.9838	0.8292	0.6827	0.5869	0.5147	0.4571	0.4115
	3.5 % Enrich.	0.9927	0.9754	0.7323	0.5779	0.4879	0.4265	0.3817	0.3490
	4.25 % Enrich.	0.9985	0.9812	0.7886	0.6346	0.5390	0.4705	0.4176	0.3777
	Small Fuel Rad.	0.9976	0.9797	0.8280	0.6804	0.5827	0.5062	0.4461	0.3964
Cold 0 ppm Decay 100hr	**Base**	1	0.9991	0.8569	0.7016	0.5857	0.4936	0.4177	0.3554
	128 I 24 W	0.9988	0.9977	0.8509	0.6959	0.5823	0.4916	0.4168	0.3556
	3.5 % Enrich.	0.9941	0.9920	0.7562	0.5798	0.4648	0.3805	0.3186	0.2738
	4.25 % Enrich.	0.9988	0.9974	0.8149	0.6468	0.5293	0.4386	0.3675	0.3123
	Small Fuel Rad.	0.9979	0.9976	0.8661	0.7172	0.6015	0.5070	0.4266	0.3594
SNF Rack Geometry	**Base**	1	0.9992	0.8505	0.6890	0.5716	0.4792	0.4032	0.3422
	128 I 24 W	0.9988	0.9981	0.8446	0.6836	0.5675	0.4780	0.4034	0.3424
	3.5 % Enrich.	0.9940	0.9920	0.7466	0.5643	0.4488	0.3650	0.3037	0.2599
	4.25 % Enrich.	0.9988	0.9975	0.8065	0.6326	0.5138	0.4241	0.3534	0.2989
	Small Fuel Rad.	0.9984	0.9976	0.8582	0.7022	0.5854	0.4906	0.4112	0.3444

Table A.III. Correlation Coefficients, c_k, Between Lattice Types (By Individual Burnup State)

		Burnup (GWd/T)							
	Lattice	**0.0**	**0.5**	**10.**	**20.**	**30.**	**40.**	**50.**	**60.**
HFP	**Base**	1	1	1	1	1	1	1	1
	128 I 24 W	0.9989	0.9990	0.9998	0.9999	0.9999	1	1	1
	3.5 % Enrich.	0.9927	0.9931	0.9831	0.9870	0.9898	0.9919	0.9939	0.9958
	4.25 % Enrich.	0.9985	0.9984	0.9963	0.9969	0.9976	0.9980	0.9984	0.9988
	Small Fuel Rad.	0.9976	0.9975	0.9971	0.9977	0.9983	0.9979	0.9981	0.9982
Cold 0 ppm Decay 100hr	**Base**	1	1	1	1	1	1	1	1
	128 I 24 W	0.9988	0.9986	0.9997	0.9999	1	1	1	1
	3.5 % Enrich.	0.9941	0.9939	0.9818	0.9836	0.9860	0.9885	0.9912	0.9937
	4.25 % Enrich.	0.9988	0.9987	0.9962	0.9963	0.9968	0.9972	0.9977	0.9983
	Small Fuel Rad.	0.9979	0.9982	0.9978	0.9981	0.9982	0.9984	0.9984	0.9985
SNF Rack Geometry	**Base**	1	1	1	1	1	1	1	1
	128 I 24 W	0.9988	0.9992	0.9997	0.9999	1	1	1	1
	3.5 % Enrich.	0.9940	0.9941	0.9817	0.9835	0.9860	0.9884	0.9910	0.9936
	4.25 % Enrich.	0.9988	0.9988	0.9961	0.9963	0.9968	0.9972	0.9977	0.9982
	Small Fuel Rad.	0.9984	0.9980	0.9977	0.9979	0.9982	0.9983	0.9986	0.9985